Ultramicroscopy 154 (2015) 57–63

Contents lists available at ScienceDirect

Ultramicroscopy

journal homepage: www.elsevier.com/locate/ultramic

On the origin of differential phase contrast at a locally charged and globally charge-compensated domain boundary in a polar-ordered material

Ian MacLaren [a,*], LiQiu Wang [a], Damien McGrouther [a], Alan J. Craven [a], Stephen McVitie [a], Roland Schierholz [b], András Kovács [c], Juri Barthel [c,d], Rafal E. Dunin-Borkowski [c]

[a] SUPA School of Physics and Astronomy, University of Glasgow, Glasgow G12 8QQ, UK
[b] Institute of Energy and Climate Research: Fundamental Electrochemistry (IEK-9), Forschungszentrum Jülich, 52425 Jülich, Germany
[c] Ernst Ruska-Centre for Microscopy and Spectroscopy with Electrons (ER-C) and Peter Grünberg Institute (PGI), Forschungszentrum Jülich GmbH, 52425 Jülich, Germany
[d] Central Facility for Electron Microscopy, RWTH Aachen University, 52074 Aachen, Germany

ARTICLE INFO

Article history:
Received 19 December 2014
Received in revised form
9 March 2015
Accepted 18 March 2015
Available online 19 March 2015

ABSTRACT

Differential phase contrast (DPC) imaging in the scanning transmission electron microscope is applied to the study of a charged antiphase domain boundary in doped bismuth ferrite. A clear differential signal is seen, which matches the expected direction of the electric field at the boundary. However, further study by scanned diffraction reveals that there is no measurable deflection of the primary diffraction disc and hence no significant free E-field in the material. Instead, the DPC signal arises from a modulation of the intensity profile within the primary diffraction disc in the vicinity of the boundary. Simulations are used to show that this modulation arises purely from the local change in crystallographic structure at the boundary and not from an electric field. This study highlights the care that is required when interpreting signals recorded from ferroelectric materials using both DPC imaging and other phase contrast techniques.

1. Introduction

In magnetic materials, it has long been known that magnetic induction (or at least the component of this perpendicular to the electron beam) results in measurable (if small) electron beam deflections in the transmission electron microscope (TEM), generally in the microradian range. Such deflections have formed the basis of a number of imaging techniques, which are collectively referred to as Lorentz microscopy and all rely on the effect of the Lorentz force on the incident electrons. One technique that is of particular interest to the current paper is differential phase contrast (DPC) imaging [1,2], whereby an electron beam is scanned across the sample and the central disc of the diffraction pattern is projected onto a quadrant detector, i.e., one that is split into four quadrants. In practice, an eight-segment octant detector, in which the central quadrant detector is surrounded by an annulus that is itself split into four sections, is used. The annular section of the detector is more sensitive to small deflections of the bright-field (BF) disc [2].

The same technique can be applied to the study of electric fields in materials. Hence, it has often been assumed that an incident electron beam would be deflected in a ferroelectrically polarised material. The electron beam deflection due to an **E**-field in a material was originally calculated by Fuchs and Liesk [3] using a simple expression based on the treatment of polarisation as it applies to a simple linear isotropic homogeneous (LIH) dielectric. The deflection angle was estimated to be

$$\gamma = \frac{1}{2U_{acc}} \frac{Pt}{(\varepsilon_r - 1)\varepsilon_o}, \quad (1)$$

where U_{acc} is the accelerating voltage, P is the polarisation and ε_r is the relative permittivity of the material. This equation was derived from the earlier textbook of Glaser [4].

The resulting value of the deflection angle can be relativistically corrected, as outlined by Lichte et al. [5], as would be necessary for accelerating voltages used in modern TEMs, i.e., principally between 60 and 300 kV at the time of writing. Such an assumption that **E**-fields due to polarisation in materials lead to beam deflection has been used in a range of studies, including recent applications of DPC imaging by Shibata et al. [6,7] and Lohr et al. [8]. Similar assumptions underlie the interpretation of images

* Corresponding author.

http://dx.doi.org/10.1016/j.ultramic.2015.03.016

recorded using other phase contrast techniques, including off-axis electron holography, from materials where internal electric fields due to polarisation are expected [5,9–11].

The counterpart to such studies of phase contrast is to perform atomic resolution imaging and to calculate the polarisation indirectly on a unit-cell by unit-cell basis from the local atomic shifts. Such measurements have been performed using both high-resolution TEM (HRTEM) and scanning TEM (STEM) imaging, and have been used to reveal details of structures including domain walls, ferroelectric vortex structures and antiferroelectric orderings [12–17]. This technique is, however, labour intensive, especially in the post-processing of the atomic resolution data, and often limited to a rather small field of view. Thus, there are clear advantages for imaging structures on the tens of nanometre scale or above using DPC imaging.

It is certainly the case that measurable DPC signals can be recorded from both ferroelectric domain structures [7] and quantum wells in polar semiconductors [8]. It is, however, not always clear whether this signal arises solely or even primarily from a beam deflection, as envisaged in the simple model described above. The present study investigates the DPC signal associated with unusual negatively-charged antiphase boundaries in doped bismuth ferrite, which have previously been characterised exhaustively using atomic-resolution techniques to reveal the structure and to infer the polarisation profile close to the boundaries [18]. The DPC signal that we record is compared with the results of a scanned diffraction investigation of these boundaries, as well as with calculated STEM diffraction patterns, in order to determine the origin of the recorded contrast.

2. Experimental

The specimen studied in this work had a composition of $(Bi_{0.85}Nd_{0.15})(Fe_{0.9}Ti_{0.1})O_3$ and was prepared as a ceramic by a mixed-oxide method, as described in detail by Kalantari et al. [19]. The material was prepared for analysis by using a modified focused ion beam (FIB) procedure. First, a section was cut through a sintered ceramic disc and polished to a very high quality surface finish using progressively finer grades of diamond paste, concluding with colloidal silica. It was then imaged uncoated using an environmental scanning electron microscope (FEI Quanta 200F). A grain that had a plane normal close to a $<100>$ axis was identified using an EDAX electron back scatter diffraction (EBSD) system and careful records were made of the area, noting the positions of useful fiducial markers (grain shapes and porosity in the ceramic). The section was then coated lightly with gold and transferred to the FIB, where the area of interest was extracted as a lamella, with a surface normal close to a $<100>$ axis in the grain of interest, as determined by comparison with the EBSD map. The grain of interest was placed approximately in the centre of the FIB section. The FIB section was carefully lifted out and attached to an Omniprobe support grid, prior to final FIB milling to a thickness of $\sim$100 nm in the area of interest. The sample was then further thinned using Ar ions in a Fischione Nanomill operated at an accelerating voltage of 500 V until the area of interest was a few nm thick at its thinnest edge, while having minimal contamination or surface damage. Comparisons of contrast in HRTEM images with simulations suggest that the thinnest areas have specimen thicknesses on the order of $\sim$4 nm. The areas used for scanned diffraction were somewhat thicker, probably on the order of 20–40 nm thick.

DPC imaging was performed using a probe-corrected JEOL ARM200F STEM equipped with a cold field emission gun (FEG) operated at 200 kV. In order to obtain controllable very low convergence angle probes that are limited in their size by diffraction and not aberrations, customised electron probes were formed with the objective lens turned off (i.e., specifically designed for Lorentz imaging [20]) using a combination of the condenser lenses and the probe aberration corrector. This configuration provides improved sensitivity in DPC imaging, as it is much simpler to detect small shifts of the probe if it only subtends a small angular range in the back focal plane. The DPC signal was recorded using a customized octant detector (Deben UK Ltd) of similar design to that described by Chapman et al. [2]. The diffraction pattern was carefully aligned to give zero differential signal in the absence of a specimen and the signal amplifiers were adjusted to give the same gain for each detector segment. Different beam convergence semi-angles (as defined by different condenser apertures) showed similar trends, with smaller condenser apertures resulting in higher sensitivity but poorer spatial resolution, while larger condenser apertures resulted in improved spatial resolution at the expense of poorer sensitivity to small disc shifts. In the example shown in this paper, a 40 μm condenser aperture was used in field-free mode to give a probe semi-angle of $\sim$1.68 mrad, which corresponds to a theoretical probe diameter of $\sim$0.75 nm according to the Abbé criterion. The camera length was adjusted so that the BF disc fell on the inner quadrants, with all of the diffraction spots outside the outer radius of these inner quadrants.

The data from the four inner quadrants was processed as pairs of differential images, corresponding to differentiation in two orthogonal directions. The images sometimes contained monotonic variations in the DPC signal across the image due to slight specimen thickness variations. These effects were compensated by subtracting an appropriate thickness wedge from the signal to produce a differential signal on a flat background. The two perpendicular differential images were then processed to produce a colour map showing both the strength and the direction of the DPC signal, according to a colour wheel [21]. (In Lorentz microscopy, such a map is related directly to the magnitude and direction of the projected transverse (i.e. in-plane) magnetic induction in the specimen). The present paper seeks to determine whether the map can be related directly to the projected transverse component of the electric field.) The colour images also contain some random colour noise in the background, which arises from a number of sources, but is always amplified in DPC imaging, since this is a differential technique involving subtraction of one large signal from another. Sources of colour noise can include surface roughness, specimen thickness and orientation changes, as well as surface contamination and local electron beam induced charging. Since the sample was imaged uncoated to maximise any electric field effects, local charging of surface features is likely to be present.

Scanned diffraction data was recorded on a Gatan Orius charge-coupled device (CCD) camera using the Gatan Diffraction Imaging plug-in for DigitalMicrograph (Gatan Inc., Pleasanton, CA). A probe semi-angle of $\sim$1.35 mrad was obtained by using a 30 μm condenser aperture in Lorentz STEM mode, as described above, corresponding to a probe size of $\sim$1 nm.

Simulations of diffraction patterns were performed for appropriately constructed supercells using *Dr. Probe* software [22]. Diffraction patterns were calculated using a multislice approach for specimen thicknesses in 12 unit cell (4.76 nm) steps up to a specimen thickness of 28.56 nm. Results are shown below for a specimen thickness of 23.8 nm (but similar trends are seen for all thicknesses). In all cases, an accelerating voltage of 200 kV and a probe semi-angle of 1.35 mrad were used, in order to match the experimental conditions.

3. Results

DPC STEM images were observed to show clear signals at antiphase boundaries. Fig. 1 shows a representative example. In

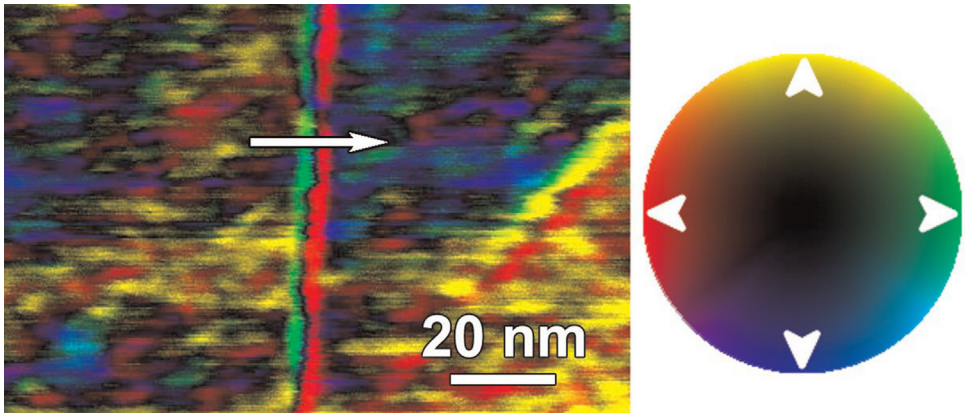

Fig. 1. Differential phase contrast signal recorded from an antiphase boundary in doped bismuth ferrite. The direction and strength of the differential signal are indicated by colours, according to the colour wheel shown. A signal is observed in the left–right direction close to the boundary, which changes sign abruptly at the boundary. The arrow shows the approximate position and direction of the profile shown in Fig. 3 below. (For interpretation of the references to color in this figure legend, the reader is referred to the web version of this article)

addition to the prevalent colour noise that is normally present when using such differential techniques, a strong and consistent DPC signal pointing to the right is observed immediately to the left of the boundary, decreasing to zero at the boundary core, before increasing to a signal of similar magnitude pointing to the left on the right of the boundary. If this signal were coming from disc shifts, then it would correspond to peak disc displacements of the order of 5 to 6 μrad. This signal could be interpreted as suggesting the presence of an **E**-field on each side of the boundary, pointing towards the boundary core. This conclusion would suggest that the boundary is negatively charged, which is known to be the case from previous work on atomic-resolution characterisation of the structure of such boundaries and the polarisation of the surrounding perovskite [18].

When scanned diffraction is performed on a similar antiphase boundary, it is immediately noticeable that the diffraction discs do not move measurably and that simple deflection of the diffraction discs is not responsible for the DPC signal. A set of diffraction discs from one such scan is shown in Fig. 2. In using phase correlation of all the discs, no detectable disc shift was identified. The sensitivity of this measurement would have been sufficient to detect shifts of the disc centroid of better than 0.1 pixels, indicating that any disc deflection could not have exceeded 1.3 μrad without being detected. In contrast, the relativistically corrected version of equation [1], as quoted by Lichte et al. [5], would have predicted a beam deflection of ~20 μrad for a sample thickness of 20 nm, a dielectric constant of ~400 [19], a peak polarisation of 0.6 Cm^{-2} [18] and an accelerating voltage of 200 kV. It is thus clear that disc deflection cannot explain the DPC signal recorded from boundaries in this polar ordered dielectric.

Whilst there is a certain intensity gradient across the disc, probably arising from a slight mistilt of the specimen away from an edge-on orientation of the boundary, it is noticeable that the contrast within the diffraction discs changes as the probe is scanned across the boundary. The manner in which this contrast changes through the scan correlates with the differential signal seen in the DPC images. In order to confirm that this intensity variation within the discs on scanning correlates with the DPC signal, a synthetic DPC linescan was calculated by using the difference between the lower right and top left of each disc, as shown in Fig. 3. This linescan has the same form of signal as that seen in the DPC image shown in Fig. 1(a profile of the *right-left* DPC signal for part of the boundary in Fig. 1 is also shown in Fig. 3), with a clear dip to the left of the boundary, a clear peak to the right of the boundary and a very similar length-scale of the differential signal. Thus, it is clear that in this case the DPC signal is caused predominantly by contrast variations within the primary diffraction disc.

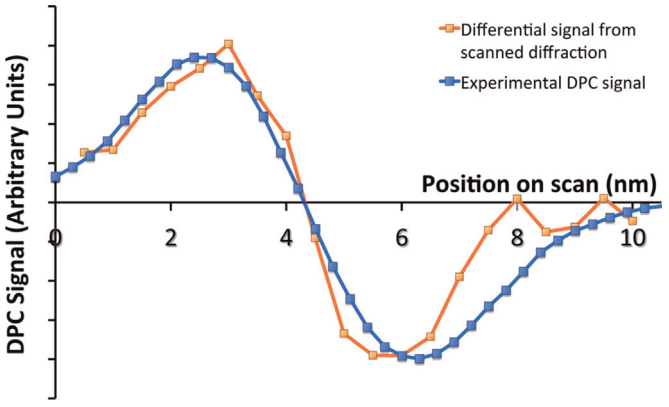

Fig. 3. Synthetic DPC linescan calculated from the diffraction patterns shown in Fig. 2 (orange), compared with the *right–left* DPC signal across the part of the boundary shown in Fig. 1 (blue). (For interpretation of the references to color in this figure legend, the reader is referred to the web version of this article).

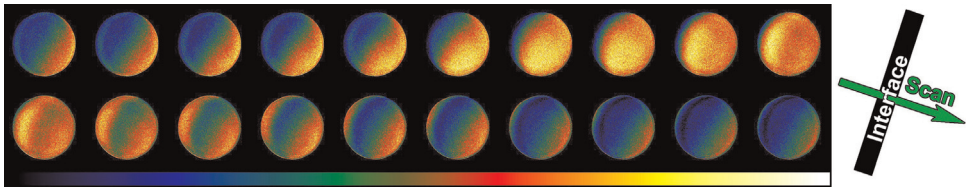

Fig. 2. Scanned diffraction discs recorded across an antiphase domain boundary of the same type as that shown in Fig. 1, shown in left-to-right order on the false-colour scale shown in the bar. The twenty discs shown were recorded with a spacing of 0.5 nm. The centre of the boundary is approximately at disc 8 or 9. As noted in the text, the position of the disc is essentially fixed.

4. Discussion

The lack of an observed disc shift in diffraction patterns recorded from a ferroelectric or polar-ordered material makes sense from the viewpoint of the theory of ferroelectrics. In a simple dielectric material, the **D** field arising from the charges is mostly screened by the presence of polarisation, such that **E** is small:

$$D=\varepsilon_0 E+ P. \quad (2)$$

For the simple idealised case of a LIH dielectric, the following equations apply:

$$P=(\varepsilon_r - 1)\varepsilon_0 E \quad (3a)$$

$$D=\varepsilon_r \varepsilon_0 E \quad (3b)$$

$$E=\frac{P}{(\varepsilon_r - 1)\varepsilon_0}. \quad (3c)$$

Eq. 3a simply relates the polarisation of the material to the strength of the applied electric field, **E**, yielding a simplified expression for **D** in terms of **E** (Eq. 3b). Eq. 3c provides the justification for the often-quoted Eq. 1. These equations have also provided the basis for the classical interpretation of electron holographic phase images recorded from dielectrics [9,10]. However, a key point has been neglected in prior attempts to understand DPC images and electron holographic phase images recorded from ferroelectrics, which are materials that support spontaneous polarisation. For ferroelectric materials imaged in the absence of an applied field, there will always be a remanent polarisation locally in each domain. In this case, $\mathbf{E}=0$, while $\mathbf{P}=\mathbf{D}$. It should therefore be clear that any ferroelectric will have no **E** field within the material in the absence of an applied field (although **E** fields may be observed as stray fields outside the specimen, or at charged domain boundaries and grain boundaries, due to unbalanced surface charges). For this reason, the correct interpretation of either DPC images or electron holographic phase images recorded from ferroelectrics or other polar-ordered materials cannot proceed from any model that has free **E** fields in the material. While it is undeniable that there is contrast present in DPC images and in electron holographic phase images recorded from ferroelectric materials [5–8,11–23,24], the interpretation of this contrast is not straightforward. It should be noted that Szwarcman et al. recently published a careful electron holography study of single and multiple domain $BaTiO_3$ nanocrystals, in which they concluded that a phase gradient was associated with ferroelectric ordering, but were unable to establish whether it arose from internal fields or diffraction effects [23].

In the present work, the structural changes that occur in the vicinity of the negatively charged antiphase boundaries are already well understood. There is a significant polarisation of the material up to a distance of approximately 5–7 unit cells on either side of the boundary – with a peak value close to 1 cm^{-2}. This is coupled to a significant tetragonal distortion of the perovskite cells from a bulk pseudocubic parameter of about 3.965 Å to a boundary value of about 4.3 Å [18]. The decay of the polarisation with distance probably occurs due to the presence of excess Ti^{4+} dopants in the $BiFeO_3$ in this region, which results in a state where **P** decays to zero and the **E**-field is zero in accordance with Gauss' law:

$$\nabla. D= \varepsilon_0 \nabla. E+ \nabla. P= \rho_c, \quad (4)$$

where ρ_c is the free charge density, in this case arising from the excess Ti^{4+}. Such a structure almost certainly formed during sintering of the ceramic [18] to minimise any long-range fields. Thus, there is local stabilisation of a pseudotetragonal, polar-ordered phase [18] in a material that would otherwise be stable in an antiferroelectric state with a structure closely related to $PbZrO_3$ [19,25]. As shown previously, this pseudotetragonal phase is closely related to the widely-studied *T*-phase of $BiFeO_3$, which can be stabilized by compressive in-plane strain [26]. The electrostatics of this structural model are summarised in more detail in the Supplementary Material. As a consequence of the polarisation to either side of the boundary, the structure is highly non-centrosymmetric in this region. It is well known that the breaking of centrosymmetry in real space results in the appearance of asymmetry between opposite diffraction spots in a diffraction pattern [27]. This effect has previously been used to study polar ordering in both semiconductors [28–31] and ferroelectrics [32]. Theoretically, it occurs through a breaking of Friedel's law, which is obeyed in the case of kinematical diffraction and would lead to the diffraction pattern of a non-centrosymmetric structure being indistinguishable from a centrosymmetric one. In practice, dynamical diffraction is dominant in all but the very thinnest of specimens (typically < 5 nm) and so Friedel's law is almost always broken for real polar specimens observed in the electron microscope. This situation should not, however, cause any change within the BF disc, which should have the symmetry of the Laue group (i.e., Friedel's law should be obeyed for the BF disc, except with tilted illumination) [27]. This behaviour can be confirmed using Bloch wave simulations [33], as shown in the Supplementary Material. Clearly, a centrosymmetric BF disc will give no DPC signal, unless it is deflected by an **E** or **B** field.

Furthermore, any local change in density, crystallographic strain, crystallographic orientation or specimen thickness at the interface will also cause the appearance of a differential signal in the immediate locality [9]. For the boundary in question, the density at its centre is expected to be reduced when compared to that in the bulk material. Even for a simple head-to-head or tail-to-tail charged domain wall, local atomic movements will cause a noticeable local change in density close to the interface. Such changes in density were previously inferred to be the prime contributor to phase contrast recorded from 24° tilt boundaries in $SrTiO_3$, without any need to invoke space charge or electric fields [34].

In order to separate these effects, simulations of convergent beam electron diffraction patterns were performed for pseudotetragonal $BiFeO_3$ with a polarisation of 1 cm^{-2} arranged at a head-to-head domain wall. (The supercell for such a model is easier to construct than one for the actual boundary, although comparable results were seen for a crude simulation of a supercell of the actual antiphase boundary structure and is shown in Figure S3 of the Supplementary Material). Since the structure model was calculated using neutral atom scattering factors, the results show the effects on electron diffraction of the screened Coulomb potential of the atomic core charges alone. Local electric fields due to the polarisation are thus not included. The patterns were simulated in 2 nm steps starting 8 nm to the left of the boundary (as illustrated in Figure S3 of the Supplementary Material). Thus, the polarisation vector should point to the right for the first four patterns, the domain wall should be at the fifth pattern and the final four patterns should have a polarisation vector pointing to the left; this is exactly what is seen in our simulations in Fig. 4. As has previously been observed in both experiments and simulations of polarised materials, there is a strong left–right contrast asymmetry in the first order diffraction spot [29–35], with the brighter side indicating the polarisation direction. In the patterns furthest from the boundary, there is almost no contrast asymmetry in the primary disc. This is typical of patterns simulated for large crystals of ferroelectric materials containing no domain boundary [27] and agrees with simulations presented in the Supplementary Material. As the probe is moved towards the boundary from the left, a bright feature enters the primary disc from the right, gradually moving to

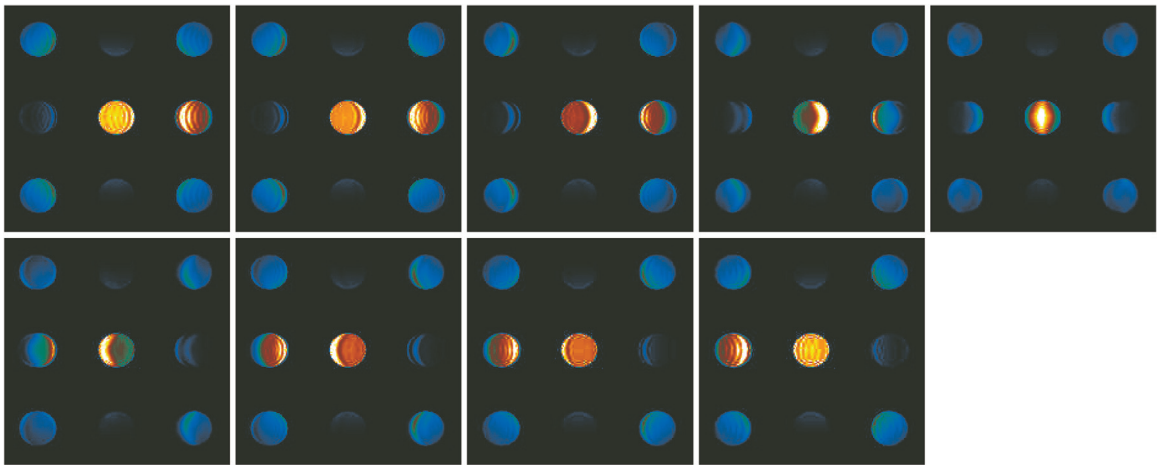

Fig. 4. Simulations of diffraction patterns calculated for a specimen thickness of ~20 nm, a probe convergence semi-angle of 1.35 mrad and an accelerating voltage of 200 kV for a head-to-head domain boundary constructed from a pseudotetragonal $BiFeO_3$ unit cell with a polarisation of 1 Cm^{-2} (i.e., similar to the peak polarisation in our material). These were calculated at 2 nm intervals whilst scanning across the boundary, with the 5th CBED pattern being exactly at the boundary.

the centre. It reaches the centre when the beam is at the boundary and then moves to the left once the beam has passed the boundary. This is exactly the behaviour seen in our experiment, as shown in Fig. 2. Thus, it is clear that a large part of the contrast that is seen in the primary diffraction disc is simply a consequence of diffraction effects arising from the presence of the boundary.

As a test, the same situation was simulated for a tail-to-tail domain boundary. The asymmetry of the first order diffraction spots was reversed, as expected, but the asymmetry in the primary disc was exactly the same as in Fig. 4, showing that this effect can arise purely from the presence of the boundary, without any need to include the effects of electric fields. Thus, the DPC signal observed in Fig. 1 can be explained by diffraction contrast effects alone, without any need for an explanation that includes electric fields within the material.

In the work described here, care was taken to use a small convergence angle for the probe to ensure that the diffraction discs did not overlap for perfect crystal. If, however, the diffraction discs are allowed to overlap with the primary disc, then the contrast asymmetries in those diffraction discs (which are prominent in the simulations shown in Fig. 4 and have previously been noted in other studies, such as that of Spellward and Preston [29]) will contribute to the DPC signal, depending on the collection angle used for the DPC quadrants. This overlap may explain at least part of the DPC contrast attributed to electric fields in other studies [7,8], especially where the convergence angles are high enough to give a resolution of much better than 1 nm and the discs overlap. It should be noted, at this point, that it should be possible to separate the effects of asymmetry within the BF disc, which arises mainly from the boundary itself, from the effects of polarisation on the crystal structure, which mainly causes asymmetry between opposite diffraction spots, by appropriate examination of scanned diffraction data. It may therefore be possible to explicitly map both effects separately by suitable processing of a scanned diffraction dataset. Similarly, using the annular DPC setup it should be possible to ensure that only the diffraction discs fall on the annular detector quadrants and the BF disc falls exclusively on the inner quadrants, resulting in the simultaneous collection of DPC signals sensitive to polarisation and boundary structure. Consequently, polarisation mapping using DPC imaging or scanned diffraction is highly feasible, especially by making use of scanned diffraction in combination with faster direct electron detectors.

There are, of course, other systems where electric fields exist in materials that are not ferroelectric but more closely approximate a linear dielectric, such as *p-n* junctions or quantum wells in semiconductors. In these materials, it is also possible that diffraction contrast arising from non-centrosymmetry and/or sharp interfaces is still a major contributor to DPC and electron holographic signals, and not the **E** field alone. Since there are minimal changes in density at a *p-n* junction in a single semiconductor, it is likely that diffraction effects are minimal in this case. On the other hand, in quantum wells and heterostructures, material changes at interfaces may be expected to cause significant diffraction contrast effects. Clearly, in order to understand any DPC or electron holographic phase contrast signal, scanned diffraction investigations are of great benefit. As noted previously by Ravikumar et al. [9], diffraction contrast effects at boundaries can result in the misinterpretation of holographic phase images. Nevertheless, in principle, it is clear that a number of effects may be happening simultaneously in such cases, including disc shifts, changes in asymmetry between opposed diffraction spots and changes within the bright field disc. With care and using scanned diffraction, it would be possible to separate these effects.

Additional complications arise when the material meets a surface or interface. In such cases, the correct boundary conditions have to be observed, resulting in changes in the **E**, **P** and **D** field distribution in the material. For a free surface to vacuum, this situation is expected to result in a fringing **E** field that can deflect the diffraction discs, as well as changing the polarisation distribution in the material. It might be expected that one could image the fringing **E** fields using DPC imaging or electron holography. Unfortunately, the surfaces of thin samples prepared for electron microscopy are often damaged by the preparation process – this already applies for samples prepared by Ar ion milling and is typically worse for samples prepared using Ga ions in a focused ion beam instrument. This damage can lead to local conductivity of the surface that quenches the stray fields, or the creation of surface electronic states that pin the Fermi level at specific positions and thus alter the electronic structure of the material within a few nm of the surface. Thus, stray fields outside ferroelectrics may well be more difficult to observe than would be desirable. More significant effects may happen if the dielectric material is in contact with a metal or a good electrical conductor. This situation can result in total quenching of all lateral components of the field at the interface and can be calculated by the method of image charges [36,37]. Tomographic reconstruction of the potential is possible in some cases in order to separate surface effects from bulk effects in a *p-n* junction and to see truly bulk-like behaviour [38].

In the particular case of semiconductors, **E**-fields associated with *p-n* junctions and quantum wells are a topic of significant technological interest. The surfaces of TEM samples of such

materials usually display quenching of electric fields, both due to the presence of surface states and due to the effects of specimen preparation [39]. A quantitative interpretation of phase contrast may also require simulations performed using specialist finite element software [40,41]. It is nevertheless the case, even here, that polarisation of the semiconductor and the presence of interfaces may add diffraction contrast to the list of effects contributing to the signal, as indicated above.

It should be noted that electric fields in free space do give rise to significant and measureable shifts of diffraction discs. In forthcoming work, we will present data showing disc deflections of tens of microradians as a consequence of electric fields in free space and we will discuss the usefulness of scanned diffraction for characterising free space electric field distributions.

It is thus clear that detailed quantitative differential phase contrast or electron holographic studies of such materials benefit from studies of scanned diffraction in order to provide an unambiguous interpretation of the contrast. In some materials, notably ferroelectrics, no significant disc shifts are observed and the signal arises primarily from diffraction effects. In the case of dielectrics examined under an applied field or semiconductor junctions, there may be a combination of a disc deflection and asymmetries within the diffraction pattern due to polarisation or interfaces. Which is the dominant effect needs to be examined in each case before any unambiguous interpretation of experimental data is possible.

5. Conclusions

Differential phase contrast signals are observed at charged antiphase boundaries in a Nd,Ti co-doped $BiFeO_3$ ceramic. The signals are similar in magnitude but have opposite signs on either side of the boundary. Scanned diffraction experiments performed on the same boundaries show no evidence of disc deflection by electric **E**-fields. The intensity distribution within the discs does, however, depend on the position of the beam with respect to the boundary and changes as one scans across the boundary, in a way that explains the DPC results. This lack of disc movement is in accordance with predictions for this case, where the **E**-field should be zero and there should be a gradual reduction of polarisation going away from the boundary due to excess Ti^{4+} in the perovskite. The same would apply for a ferroelectric in the absence of an externally applied field, since there should be zero **E**-field within each grain, with the **P-** and **D**-fields balancing exactly. In the present study, the differential signal arises primarily from to a local structural change at the interface (and a consequent change in local density), leading to contrast within the primary diffraction disc. We show that differential signals could also arise from asymmetry between opposed first order reflections in the diffraction pattern due to the effects of polarisation on the crystal symmetry. Our results suggest that the majority of DPC and electron holographic signals that have been recorded from similar boundaries in ferroelectric materials may have arisen from diffraction effects associated with local changes in density, crystallographic orientation, specimen thickness or non-centrosymmetry of the unit cell. Further investigations are necessary to understand the behaviour of diffraction discs in linear dielectrics with low dielectric constants. It is expected that both disc deflections and diffraction contrast may then contribute to the signal. Consequently, careful scanned diffraction studies of the effects of polarisation fields are essential for a better understanding of DPC and electron holographic signals recorded from dielectric materials and nanostructures.

Acknowledgements

The authors gratefully acknowledge the support of the EPSRC for this work through the provision of a PhD studentship for LQW. This work was only possible through the provision of a suitable sample by Prof. Ian M. Reaney at the University of Sheffield produced in previous EPSRC projects (EP/G069069/1 and EP/G005001/1). We are grateful to the University of Glasgow and SUPA for the provision of the MagTEM facility that was used for this work, as well as to JEOL and CEOS GmbH for their help in developing the aberration-corrected, low convergence angle, magnetic-field-free imaging modes used in this work. We are also grateful to Mr Peter Chung and Prof Martin Lee of the University of Glasgow for assistance with the ESEM/EBSD system used in the initial stages of sample preparation.

Appendix A. Suplementary Information

Supplementary data associated with this article can be found in the online version at http://dx.doi.org/10.1016/j.ultramic.2015.03.016.

References

[1] J.N. Chapman, P.E. Batson, E.M. Waddell, R.P. Ferrier, Direct determination of magnetic domain-wall profiles by differential phase-contrast electron-microscopy, Ultramicroscopy 3 (1978) 203–214.
[2] J.N. Chapman, I.R. McFadyen, S. McVitie, Modified differential phase-contrast lorentz microscopy for improved imaging of magnetic-structures, IEEE Trans. Magn. 26 (1990) 1506–1511.
[3] E. Fuchs, W. Liesk, Elektronenmikroskopische Beobachtung von Domanenkonfigurationen und von Umpolarisationsvorgangen in dunnen BaTiO3-Einkristallen, J. Phys. Chem. Solids 25 (1964) 845.
[4] W. Glaser, Grundlagen der Elektronenoptik, Springer-Verlag, Vienna, 1952.
[5] H. Lichte, M. Reibold, K. Brand, M. Lehmann, Ferroelectric electron holography, Ultramicroscopy 93 (2002) 199–212.
[6] N. Shibata, Y. Kohno, S.D. Findlay, H. Sawada, Y. Kondo, Y. Ikuhara, New area detector for atomic-resolution scanning transmission electron microscopy, J. Electron Microsc. 59 (2010) 473–479.
[7] N. Shibata, S.D. Findlay, Y. Kohno, H. Sawada, Y. Kondo, Y. Ikuhara, Differential phase-contrast microscopy at atomic resolution, Nat. Phys. 8 (2012) 611–615.
[8] M. Lohr, R. Schregle, M. Jetter, C. Wachter, T. Wunderer, F. Scholz, J. Zweck, Differential phase contrast 2.0-Opening new "fields" for an established technique, Ultramicroscopy 117 (2012) 7–14.
[9] V. Ravikumar, R.P. Rodrigues, V.P. Dravid, Space-charge distribution across internal interfaces in electroceramics using electron holography.1. Pristine grain boundaries, J. Am. Ceram. Soc. 80 (1997) 1117–1130.
[10] V. Ravikumar, R.P. Rodrigues, V.P. Dravid, Space-charge distribution across internal interfaces in electroceramics using electron holography.2. Doped grain boundaries, J. Am. Ceram. Soc. 80 (1997) 1131–1138.
[11] T. Matsumoto, M. Koguchi, K. Suzuki, H. Nishimura, Y. Motoyoshi, N. Wada, Ferroelectric 90 degrees domain structure in a thin film of $BaTiO_3$ fine ceramics observed by 300 kV electron holography, Appl. Phys. Lett. 92 (2008) 3.
[12] C.L. Jia, S.B. Mi, K. Urban, I. Vrejoiu, M. Alexe, D. Hesse, Atomic-scale study of electric dipoles near charged and uncharged domain walls in ferroelectric films, Nat. Mater. 7 (2008) 57–61.
[13] C.L. Jia, V. Nagarajan, J.Q. He, L. Houben, T. Zhao, R. Ramesh, K. Urban, R. Waser, Unit-cell scale mapping of ferroelectricity and tetragonality in epitaxial ultrathin ferroelectric films, Nat. Mater. 6 (2007) 64–69.
[14] C.T. Nelson, B. Winchester, Y. Zhang, S.J. Kim, A. Melville, C. Adamo, C. M. Folkman, S.H. Baek, C.B. Eom, D.G. Schlom, L.Q. Chen, X.Q. Pan, Spontaneous vortex nanodomain arrays at ferroelectric heterointerfaces, Nano Lett. 11 (2011) 828–834.
[15] I. MacLaren, R. Villaurrutia, B. Schaffer, L. Houben, A. Pelaiz-Barranco, Atomic-scale imaging and quantification of electrical polarisation in incommensurate antiferroelectric lanthanum-doped lead zirconate titanate, Adv. Func. Mater. 22 (2012) 261–266.
[16] A. Lubk, M.D. Rossell, J. Seidel, Q. He, S.Y. Yang, Y.H. Chu, R. Ramesh, M.J. Hytch, E. Snoeck, Evidence of sharp and diffuse domain walls in $BiFeO_3$ by means of unit-cell-wise strain and polarization maps obtained with high resolution scanning transmission electron microscopy, Phys. Rev. Lett. 109 (2012).
[17] G. Catalan, A. Lubk, A.H.G. Vlooswijk, E. Snoeck, C. Magen, A. Janssen, G. Rispens, G. Rijnders, D.H.A. Blank, B. Noheda, Flexoelectric rotation of polarization in ferroelectric thin films, Nat. Mater. 10 (2011) 963–967.
[18] I. MacLaren, L.Q. Wang, O. Morris, A.J. Craven, R.L. Stamps, B. Schaffer, Q.

M. Ramasse, S. Miao, K. Kalantari, I. Sterianou, I.M. Reaney, Local stabilisation of polar order at charged antiphase boundaries in antiferroelectric $(Bi_{0.85}Nd_{0.15})(Ti_{0.1}Fe_{0.9})O_3$, APL Mater. 1 (2013) 021102.
[19] K. Kalantari, I. Sterianou, S. Karimi, M.C. Ferrarelli, S. Miao, D.C. Sinclair, I. M. Reaney, Ti-doping to reduce conductivity in $Bi_{0.85}Nd_{0.15}FeO_3$ ceramics, Adv. Func. Mater. 21 (2011) 3737–3743.
[20] D. McGrouther, M.J. Benitez, S. McFadzean, S. McVitie, Development of aberration corrected differential phase contrast (DPC) STEM, JEOL News 49 (2014) 2–10.
[21] C.W. Sandweg, N. Wiese, D. McGrouther, S.J. Hermsdoerfer, H. Schultheiss, B. Leven, S. McVitie, B. Hillebrands, J.N. Chapman, Direct observation of domain wall structures in curved permalloy wires containing an antinotch, J. Appl. Phys. 103 (2008) 093906.
[22] J. Barthel, Dr Probe, STEM simulation software, (http://www.er-c.org/barthel/drprobe), 2014,.
[23] D. Szwarcman, A. Lubk, M. Linck, K. Vogel, Y. Lereah, H. Lichte, G. Markovich, Ferroelectric effects in individual $BaTiO_3$ nanocrystals investigated by electron holography, Phys. Rev. B 85 (2012) 134112.
[24] D. Szwarcman, S. Prosandeev, L. Louis, S. Berger, Y. Rosenberg, Y. Lereah, L. Bellaiche, G. Markovich, The stabilization of a single domain in free-standing ferroelectric nanocrystals, J Phys.: Condens. Mater. 26 (2014) 8.
[25] I. Levin, S. Karimi, V. Provenzano, C.L. Dennis, H. Wu, T.P. Comyn, T. J. Stevenson, R.I. Smith, I.M. Reaney, Reorientation of magnetic dipoles at the antiferroelectric-paraelectric phase transition of $Bi_{1-x}Nd_xFeO_3$ ($0.15 <= x <= 0.25$), Phys. Rev. B 81 (2010) 020103.
[26] R.J. Zeches, M.D. Rossell, J.X. Zhang, A.J. Hatt, Q. He, C.H. Yang, A. Kumar, C. H. Wang, A. Melville, C. Adamo, G. Sheng, Y.H. Chu, J.F. Ihlefeld, R. Erni, C. Ederer, V. Gopalan, L.Q. Chen, D.G. Schlom, N.A. Spaldin, L.W. Martin, R. Ramesh, A Strain-Driven Morphotropic Phase Boundary in $BiFeO_3$, Science 326 (2009) 977–980.
[27] B.F. Buxton, J.A. Eades, J.W. Steeds, G.M. Rackham, Symmetry of electron-diffraction zone axis patterns, Philos. Trans. R. Soc. A: Math. Phys. Eng. Sci. 281 (1976) 171.
[28] K. Ishizuka, J. Taftø, Quantitative-analysis of CBED to determine polarity and ionicity of ZnS-type crystals, Acta Crystallogr. Sect. B: Struct. Commun. 40 (1984) 332–337.
[29] P. Spellward, A.R. Preston, Determination of the polarity of twins in epitaxial cadmium telluride using convergent beam electron-diffraction, Inst. Phys. Conf. Ser. (1988) 29–30.
[30] K. Marthinsen, T. Lindheim, R. Hoier, Non-centrosymmetry effects and polarity determination in III-V semiconductors, Acta Crystallogr. A 53 (1997) 366–375.
[31] J.M. LeBeau, S.D. Findlay, L.J. Allen, S. Stemmer, Position averaged convergent beam electron diffraction: theory and applications, Ultramicroscopy 110 (2010) 118–125.
[32] C. Guo, H.M. Zou, S.Z. Pu, M.Y. Li, J.F. Cao, Polarity determination of ferroelectric LiNbO3 crystals and BiFeO3 thin films by the convergent beam electron diffraction technique, Mater. Charact. 61 (2010) 859–865.
[33] K. Tsuda, M. Tanaka, Refinement of crystal structural parameters using two-dimensional energy-filtered CBED patterns, Acta Crystallogr. A 55 (1999) 939–954.
[34] Z.G. Mao, R.E. Dunin-Borkowski, C.B. Boothroyd, K.M. Knowles, Direct measurement and interpretation of electrostatic potentials at 24 degrees 001 tilt boundaries in undoped and niobium-doped strontium titanate bicrystals, J. Am. Ceram. Soc. 81 (1998) 2917–2926.
[35] J.M. LeBeau, A.J. D'Alfonso, N.J. Wright, L.J. Allen, S. Stemmer, Determining ferroelectric polarity at the nanoscale, Appl. Phys. Lett. 98 (2011).
[36] R.E. Dunin-Borkowski, W.O. Saxton, The electrostatic contribution to the forward-scattering potential at a space charge layer in high-energy electron diffraction.2. Fringing fields, Acta Crystallogr. A 53 (1997) 242–250.
[37] R.E. Dunin-Borkowski, W.O. Saxton, W.M. Stobbs, The electrostatic contribution to the forward-scattering potential at a space charge layer in high-energy electron diffraction.1. Theory neglecting the effects of fringing fields, Acta Crystallogr. A 52 (1996) 705–711.
[38] A.C. Twitchett-Harrison, T.J.V. Yates, R.E. Dunin-Borkowski, P.A. Midgley, Quantitative electron holographic tomography for the 3D characterisation of semiconductor device structures, Ultramicroscopy 108 (2008) 1401–1407.
[39] A.C. Twitchett, R.E. Dunin-Borkowski, R.F. Broom, P.A. Midgley, Quantitative electron holography of biased semiconductor devices, J. Phys.: Condensed Matter 16 (2004) S181–S192.
[40] P.K. Somodi, A.C. Twitchett-Harrison, P.A. Midgley, B.E. Kardynal, C.H. W. Barnes, R.E. Dunin-Borkowski, Finite element simulations of electrostatic dopant potentials in thin semiconductor specimens for electron holography, Ultramicroscopy 134 (2013) 160–166.
[41] A. Pantzer, A. Vakahy, Z. Eliyahou, G. Levi, D. Horvitz, A. Kohn, Dopant mapping in thin FIB prepared silicon samples by off-axis electron holography, Ultramicroscopy 138 (2014) 36–45.